REVISTA MATÉRIA V.28 N.3
ISSN 1517-7076 articles e20230115, 2023

Fracture mechanics analysis of a fatigue failure of a parabolic spring

Mirco Daniel Chapetti[1], Bojan Senčič[2], Nenad Gubeljak[3]

[1]Universidad Nacional de Mar del Plata, Consejo Nacional de Investigaciones Científicas y Técnicas, Instituto de Investigaciones en Ciencia y Tecnología de Materiales, Laboratorio de Mecánica Experimental. Av. Colón 10850, 7600, Mar del Plata, Argentina.

[2]Steelwork company, Štore Steel d.o.o.. Železarska cesta 3, 3220, Štore, Slovenia.

[3]University of Maribor, Faculty of Mechanical Engineering. Smetanova ul. 17, 2000, Maribor, Slovenia.

e-mail: mchapetti@fi.mdp.edu.ar, bojan.sencic@store-steel.si, nenad.gubeljak@um.si

ABSTRACT

This study analyzed the fatigue failure of a parabolic spring made of 51CrV4 steel. A fracture mechanics approach was used to quantify the driving force and resistance for different loading configurations, inclusion sizes, and residual stresses. The analysis considered surface and internal initiation processes, including the impact of residual stresses introduced by shot peening. Key findings include the ability of the methodology to analyze the variables influencing fatigue resistance and failure configuration, the competition between surface and internal fracture processes, the limitation of residual stresses, the importance of minimizing the maximum inclusion size, and the potential for enhancing the propagation threshold for long cracks. The employed methodology facilitates not only the quantification but also the comprehension of the influence of the intrinsic material resistance on the fracture process.

Keywords: Spring; fracture mechanics; short cracks; fatigue strength estimation; small defect assessment.

1. INTRODUCTION

Fatigue failure is a common problem in spring leaves, often caused by internal inclusions [1–3]. The initiation location of the crack depends on various factors associated with the fatigue mechanism, including the weakest configuration of the material's resistance, inclusion size (acting as a crack nucleator), residual stresses, and loading conditions. Figure 1 provides visual examples of parabolic springs that experienced fatigue failure, with a sub-surface crack initiated by a non-metallic inclusion.

Thermo-mechanical treated high-strength steel grade 51CrV4 is commonly employed in the manufacturing of parabolic springs for heavy vehicles, due to its remarkable strength and the induction of high compressive residual stresses on the tension-loaded surfaces and sub-surfaces of the leaves [4]. Although improvements in steel production have resulted in a reduction in inclusion sizes and an overall increase in fatigue strength, defects with sizes of hundreds of microns can still be found. The statistical distribution of these defects in terms of size and position makes their analysis a challenging task.

Shot-peening is a common technique used to introduce high surface compressive residual stress amplitudes in bending loaded spring leaves, which can prevent fatigue crack propagation from the surface [5, 6]. When properly done, shot-peening generates high compressive residual stresses that move the fatigue crack nucleation process to the inner part of the leaf, where the effective driving force is higher.

The aim of this study was to estimate and analyze the fatigue failure of a parabolic spring made of 51CrV4 steel and compare the findings with experimental data. The analysis utilized a fracture mechanics approach and the concept of a resistance curve to quantify the applied driving force and the resistance for various loading configurations, inclusion sizes, and residual stresses. A comparison between surface and internal initiation processes was conducted, taking into account the impact of residual stresses introduced by shot-peening in the former case.

In the following section 2, the material properties of the spring, the mechanical tests conducted to characterize its fatigue life and resistance to long crack propagation, the estimations of residual stresses introduced by the shot peening process, and the fatigue testing of the springs are introduced. Then, in section 3, a fracture mechanics analysis of the two competing failure processes is performed, including estimation of resistance to

Corresponding Author: Mirco Daniel Chapetti Received on 04/04/2023 Accepted on 27/06/2023

DOI: https://doi.org/10.1590/1517-7076-RMAT-2023-0115

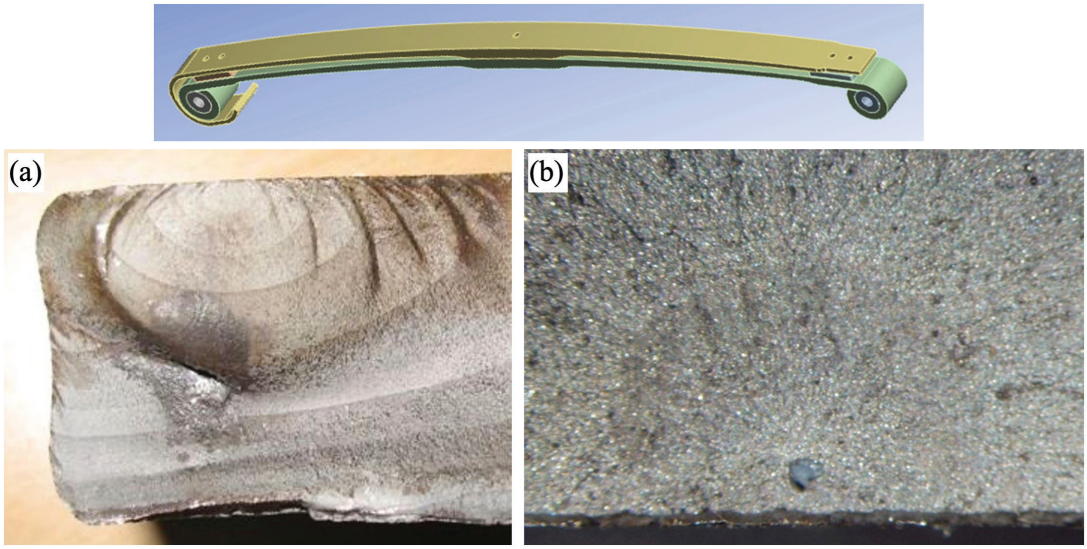

Figure 1: Examples of parabolic springs failed due to fatigue: (a) Spring fracture surface. (b) Fatigue crack initiation from a sub-surface non-metallic inclusion.

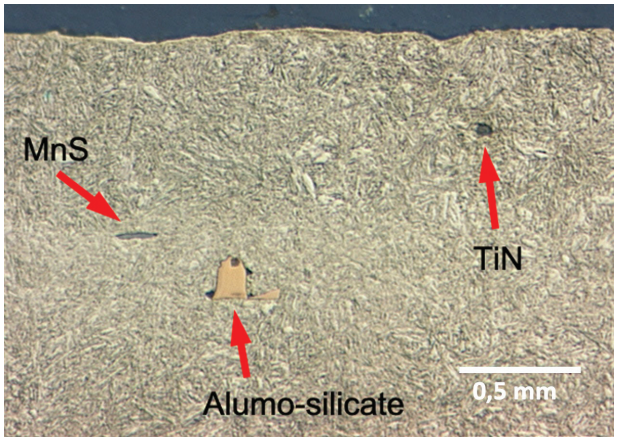

Figure 2: Details of microstructure and inclusions of the 51CrV4 spring steel.

short crack propagation and its range, driving forces in both possible initiation processes (surface and internal), and fatigue lives and fatigue limits for different configurations. Finally, conclusions are drawn, and important aspects of the obtained results are emphasized.

2. MATERIAL AND SPRING PROPERTIES, EXPERIMENTS AND RESULTS

2.1. Spring steel

The 51CrV4 spring steel is delivered to the spring producer in a hot-rolled state with a ferrite-perlite microstructure, an average grain size of d = 10 µm, and an average hardness of 430 HV (42 ± 2 HRC). Its chemical composition consists of 0.5% C, 0.3% Si, 0.95% Mn, 1% Cr, 0.15% V, and Fe.

The yield stress of the steel in its delivered condition is $\sigma_{0.2}$ = 1050 MPa, and the ultimate tensile strength is σ_U = 1270 MPa [7, 8]. The spring producer performs several manufacturing processes, including hot rolling, hot bending, eye-making, and heat treatment. The goal of the heat treatment is to obtain a fine microstructure of tempered martensite, with an average grain size of d = 5 µm and an average hardness of 590 HV (52 ± 2 HRC). The final yield stress of the steel is $\sigma_{0,2}$ = 1580 MPa, and the ultimate tensile strength is σ_U = 1670 MPa. Inclusions of MnS, Al-silicates, and TiN are present, with sizes ranging from 50 µm to 500 µm. Figure 2 displays a photograph of the microstructure with the three types of inclusions.

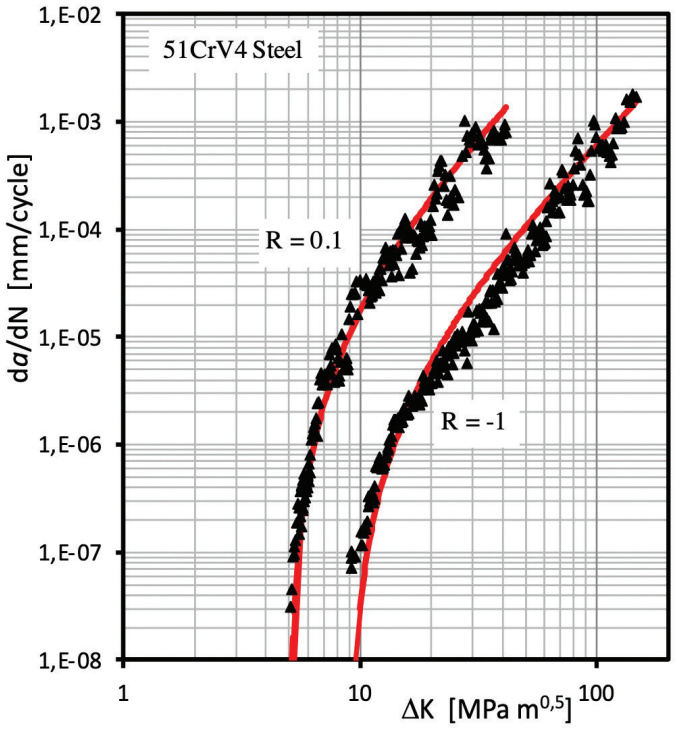

Figure 3: Fatigue crack growth results.

2.2. Fatigue endurance of the 51CrV4 steel

A common practice in ongoing material analysis is to characterize it without residual stresses to obtain reference intrinsic resistance values. However, the presence of significant defects, much larger than the microstructural size, makes it inappropriate to use experimental evaluations as reference resistances because they would reflect a configuration that includes the influence of defects on the matrix's resistance. To illustrate these concepts, we conducted a characterization of the steel in its final condition (including matrix and inclusions) using flexorotative fatigue tests. The tests were carried out on hourglass-shaped specimens at room temperature using a four-axis cantilever-type rotary bending fatigue machine with a stress ratio $R = -1$. The specimens had a grip diameter of 15 mm and a minimum diameter of 7.5 mm. To eliminate surface residual stresses, the specimens were ground and electro-polished to remove a 100 µm-thick surface layer. The experimental results were reported in reference [9], from which we obtained an endurance limit $\Delta\sigma_e = 360$ MPa.

Section 3.1 will focus on estimating and analyzing the intrinsic fatigue limit (or endurance) of the matrix. It is crucial to clarify the conceptual difference between the resistance of the matrix and the resistance of the final assembly (matrix plus defects) to appropriately apply fracture mechanics models. These models consider defects as the initial equivalent cracks that lead to the fracture process of the component.

2.3. Long fatigue crack growth properties

Fatigue crack growth properties for long cracks were obtained for stress ratios $R = -1$ and 0.1 [10]. The tests were conducted using a three-point bending configuration on specimens with dimensions of 6.5 × 16 × 100 mm and a 1.5 mm deep notch. The crack growth properties and ΔK_{thR} threshold were determined in accordance with the ASTM E-647 or ISO 12108 standard [11, 12]. Experimental values of *da/dN* vs ΔK are shown in Figure 3. The measured fatigue thresholds for long cracks were found to be $\Delta K_{thR} = 9.2$ and 5 MPa·m$^{1/2}$ for $R = -1$ and 0.1, respectively.

The properties obtained from the fatigue crack growth analysis can be applied to superficial cracks as the characterizations were performed with cracks open to the environment. However, it should be noted that the same properties can also be used for internal cracks. In such cases, it is important to consider that the resistance to crack propagation is expected to be higher, as diffusive processes and environmental damage are limited [13, 14]. Therefore, the properties obtained from the analysis of open cracks can be considered conservative for internal cracks.

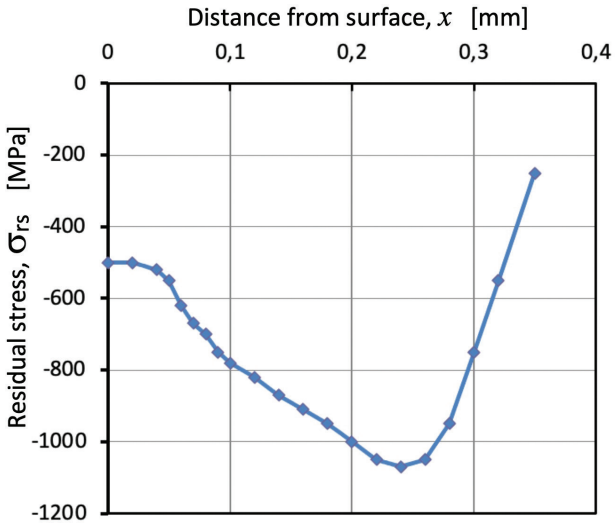

Figure 4: Residual stress distribution. Average of data taken from reference [15] is shown.

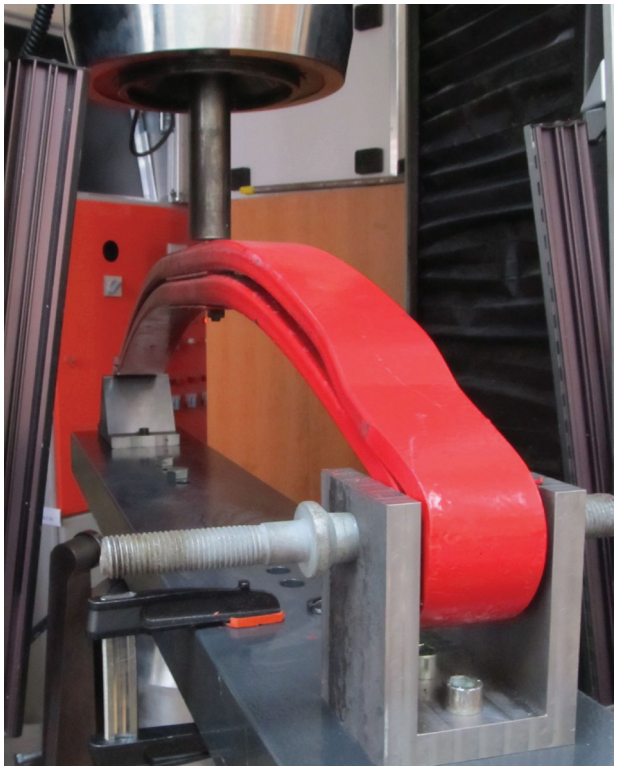

Figure 5: Fatigue test setup for spring leaves.

2.4. Residual stresses

Shot peening of the spring surface was performed using a 30 kW electric motor-powered turbine operating at a rotation speed of 3000 min^{-1}. The process utilized hard steel balls with an average diameter of 2 mm, resulting in an average exit speed of 80 m/s. The total material throughput during the process was 1149 kg/min.

The final condition of the spring leaf was used for surface measurement of residual stresses, which was performed at room temperature and ambient conditions using the X-ray diffraction method. The measured compressive residual stress on the surface in the longitudinal direction was found to be –493 ± 20 MPa. To account for the stress distribution, data reported by SCURACCHIO *et al*. in reference [15] was used as a first approximation since they reported similar values of stresses on the surface. Figure 4 shows the average distribution of values obtained by SCURACCHIO *et al*. for four different shot peening configurations. The results showed that the maximum residual stress, which is in compression, is obtained at a depth of about 0.25 mm and is equal to

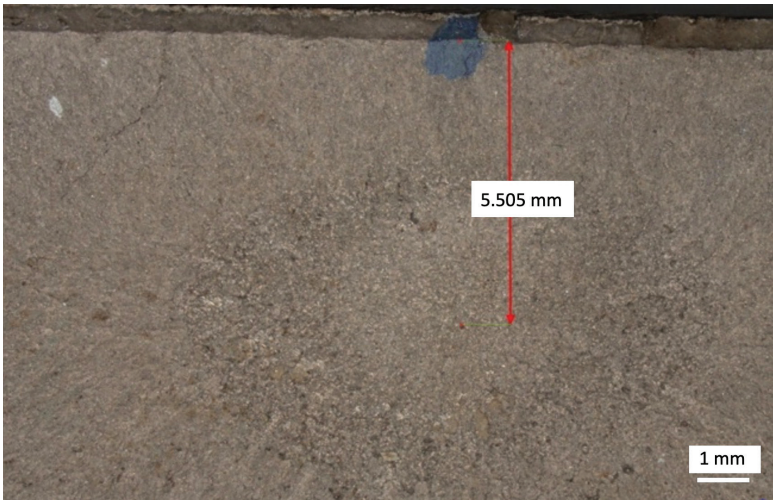

Figure 6: Fracture surface of spring #6.

Table 1: Experimental data for spring tests.

SPRING NUMBER	NUMBER OF CYCLES TO FAILURE	DEFECT SIZE, $2a_i$ [mm]	DEPTH, D [mm]
1	17052	0.089	4.07
2	71958	0.207	6.03
3	20856	0.097	4.42
4	10506	0.140	3.21
5	17652	0.184	3.99
6	42536	0.091	5.51

about 1100–1200 MPa. This value is significantly higher than the one near the surface. At greater depths, the residual stress persists in compression, ranging from –500 MPa to –800 MPa at a depth of about 0.3 mm.

With increasing depth, the stresses gradually decrease and eventually transition to positive values, creating tension to counterbalance the negative stresses and achieve a net zero force in the specified direction.

2.5. Parabolic spring fatigue testing and experimental results

Six springs were subjected to regular quality assessment tests by the manufacturer. Three-point bending tests were conducted on the springs, with a stress range of 1200 MPa at a stress ratio of $R = 0.1$ and a frequency of 1 Hz. Springs were tested under load-controlled conditions until fracture. The experimental setup is shown in Figure 5. In all cases, fracture occurred due to crack nucleation from the interior of the springs. Table 1 provides information regarding the number of fatigue cycles to failure, the size of the defect that caused failure, and the position of the defect at which nucleation occurred.

The fracture surface of spring number 6 is depicted in Figure 6, where the initiating defect leading to failure and depth of its location can be observed. The figure also reveals the size of the subcritical propagation zone of a circumferential crack, which has a propagation range of approximately 3 mm.

3. FRACTURE MECHANICS ANALYSIS

The fractures were caused by internal defects that were located at depths greater than 3 mm. Residual stresses near the surface were found to have no significant influence in this area. It is evident that the presence of residual compressive stresses prevented the nucleation of superficial cracks. Consequently, the fracture process turns into a competition between two mechanisms: superficial and internal initiation.

Initially, the range of short cracks is estimated, simplifying the analysis to a problem of long crack thresholds. Subsequently, the analysis focuses on the nucleation process of surface cracks, demonstrating their unlikelihood to occur at or below the applied nominal stress levels due to the presence of residual compressive stresses. Finally, the failure process is investigated through the propagation of cracks originating from internal defects.

3.1. Short crack range estimation

Let's analyze the transition between the threshold associated with the plain fatigue limit, $\Delta\sigma_{eR}$, and the threshold for long crack propagation, ΔK_{thR}. This transition is complex and challenging to estimate and measure experimentally due to the requirement of dealing with very small cracks in threshold configurations. Within this given crack length range, the threshold in terms of the stress intensity factor range increases from a minimum value associated with the fatigue limit to the threshold for long cracks. For further details on the analysis of this short crack range, refer to references [16–18]. To estimate the short crack regime in terms of crack length and determine if dealing with short cracks is necessary, we will use the Chapetti model [19] and the Murakami-Endo model [20, 21].

The Chapetti model estimates the threshold for crack growth as a function of crack length using the following equation [19]:

$$\Delta K_{th} = \Delta K_{dR} + \left(\Delta K_{thR} - \Delta K_{dR}\right)\left[1 - e^{-k(a-d)}\right] \qquad a \geq d \tag{1}$$

where a is the crack length, ΔK_{thR} is the threshold for long cracks for a given R ratio, d is the microstructural dimension (e.g., average grain size), and ΔK_{dR} is the microstructural threshold associated to the fatigue limit (minimum value for ΔK_{th}) given by [19]:

$$\Delta K_{dR} = Y\,\Delta\sigma_{eR}\sqrt{\pi\, d} \tag{2}$$

where $\Delta\sigma_{eR}$ is the fatigue limit (or endurance). The parameter k in Eq. (1) is a material constant given by the following expression [19]:

$$k = \frac{1}{4d}\frac{\Delta K_{dR}}{\left(\Delta K_{thR} - \Delta K_{dR}\right)} \tag{3}$$

Eq. (1) is fully defined once $\Delta\sigma_{eR}$, ΔK_{thR} and d are known. These parameters can be easily obtained from common standardized fatigue tests and metallographic analysis.

In most cases, microstructurally nucleated surface cracks are considered to be semicircular, and a value of 0.65 is typically used for Y [13, 14]. It is worth noting that the microstructural threshold also depends on the stress ratio R [13, 14, 16]. The average microstructural characteristic dimension, such as grain size, is often used to determine d. For the analyzed steel in quenched and tempered (Q+T) condition, d is equal to 5 μm. Additional information and assumptions of this model can be found in references [22] and [23].

The Murakami-Endo model [20] estimates the threshold ΔK_{th} for small cracks and defects in terms of the Vickers hardness, H_V, and the $area^{1/2}$ parameter defined as the square root of the area obtained by projecting a small defect or crack onto a plane perpendicular to the maximum principal stress. Murakami and Endo proposed the following expression to estimate the threshold stress range $\Delta\sigma_{th}$ for surface cracks and $R = -1$ [20, 21]:

$$\Delta\sigma_{th} = \frac{2.86\left(H_V + 120\right)}{\left(\sqrt{area}\right)^{1/6}} \tag{4}$$

where $area^{1/2}$ is in μm and H_V in kgf/mm², given $\Delta\sigma_{th}$ in MPa. In the case of the threshold for short crack growth in terms of the ΔK, the following expression was proposed:

$$\Delta K_{th} = 0,0033\left(H_V + 120\right)\left(\sqrt{area}\right)^{1/3} \tag{5}$$

Eqs. (4) and (5) are applicable under fully reversed loading condition, i.e. for load ratio $R = -1$. The effect of load ratio is taken into account by the model by multiplying the expressions (4) and (5) by the following factor [21]:

$$\left(\frac{1-R}{2}\right)^{\alpha} \tag{6}$$

with α given by the expression $\alpha = 0.266 + H_V \cdot 10^{-4}$ [21].

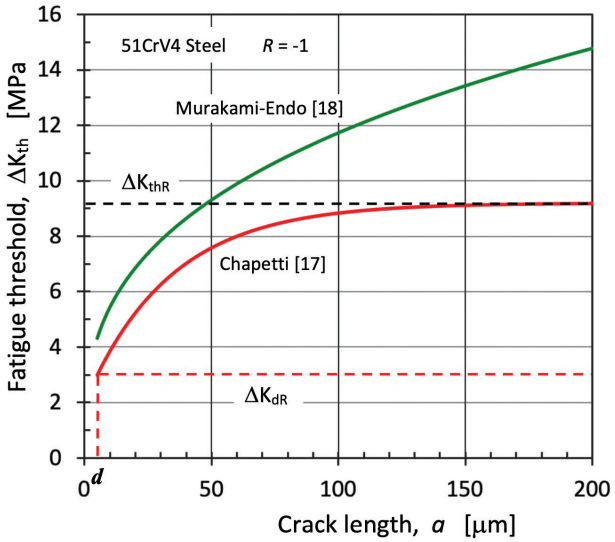

Figure 7: Resistance curves for short crack propagation estimated by using Murakami-Endo [20] and Chapetti [19] models.

An essential aspect of this model is that it proposes a constant potential relationship between the propagation threshold and the defect size. However, as the ΔK_{th} approaches the threshold for long cracks (ΔK_{thR}), it is no longer dependent on the size of the defect as it falls outside the range of short cracks (see Figure 7). Then, the threshold for long cracks defines an upper limit for the validity of the Murakami-Endo model [24].

A lower bound can be defined for the Eq. (5), given by the microstructural dimension *d*, so that a minimum ΔK_{th} associated to the fatigue limit can be defined, called ΔK_{dR} in Chapetti's model (see Eq. 2). In terms of the fatigue limit, Eq. (4) should also have a limit because a null defect size would result in an infinite fatigue limit (or zero threshold in Eq. 5). It's important to highlight the difference between the intrinsic fatigue limit of the material associated with its matrix (and therefore its hardness) and the fatigue limit of the matrix-defect combination. This is especially important in the case of high-strength steels with a high-hardness matrix and significant defect sizes relative to the microstructural dimension (in this case, $d = 0.005$ mm, and the defect size is in the range of 0.05 mm to 0.35 mm). To address this issue, a lower bound can be defined for Eq. (5), given by the microstructural dimension *d*. This lower bound allows for the definition of a minimum ΔK_{th} associated with the fatigue limit, called ΔK_{dR} in Chapetti's model (see Eq. 2). By setting the parameter $area^{1/2}$ equal to 1.253 times the average grain size *d*, that is to say, making the area equal to a semicircular surface cracks of depth *d*, we obtain:

$$\Delta K_{dR} = 0.00356\left(H_V + 120\right)d^{1/3} \tag{7}$$

With *d* in μm and H_V in kgf/mm$^{1/2}$, given ΔK_{dR} in MPa.m$^{1/2}$. In terms of stress range, we get the following expression to estimate the inherent fatigue limit (or endurance) of the matrix:

$$\Delta\sigma_{eR} = 2,653\frac{\left(H_V + 120\right)}{d^{1/6}} \tag{8}$$

For our steel (d = 5 μm, Hv = 590 kgf/mm^2), Eq. (8) gives an intrinsic fatigue limit associated to the matrix equal to 1440 MPa. When compared with the tensile strength, it is obtained that $\Delta\sigma_{eR} = 0.86\ \sigma_U$, or $\sigma_{eR} = 0.43\ \sigma_U$, an acceptable value taking into account the traditional relationship for $R = -1$ between the tensile strength and the fatigue limit associated with the natural-nucleated surface cracks. Replacing this value in Eq. (2), we get that ΔK_{dR} is equal to 3.71 MPa.m$^{1/2}$, less than half the threshold value for long cracks (ΔK_{thR} = 9.2 MPa.m$^{1/2}$). It is important to remember that Eq. (8) estimates the intrinsic resistance of the matrix of the steel without defects. The influence of the defect can then be estimated by applying the resistance curve concept, that is to say, estimating the applied nominal stress for which the ΔK applied to the analyzed defect exceeds the propagation threshold ΔK_{th} (given by Eq. 2) for the equivalent crack length.

Figure 7 shows the threshold curves estimated by the models. In the case of the Chapetti model, Eqs. (2) and (8) are used to estimate ΔK_{dR}. The short crack range covers only the first 70–100 μm of the range of defect

sizes, which spans from 50 to 350 μm. Furthermore, the Murakami-Endo model predicts a slightly smaller range of short cracks, as the threshold equals that of long cracks for defect sizes of approximately 50 μm. Thus, for the present analysis, we can conclude that only the long crack threshold needs to be considered for the entire range of defect sizes.

It could be argued that the propagation threshold should initially be equal to the minimum (ΔK_{dR}) and that its development should take place even for cracks initiated from relatively large defects. Some researchers suggest that the crack closure effect, which is considered by most of the scientific community as solely responsible for the development of the threshold, starts to develop when cracks nucleate from the defects [25–28]. However, the development rate will depend on the defect size, that is to say, it will depend on the total equivalent initial crack length involved in the configuration (defect plus crack). Once the nucleated crack starts to grow, the stress field at the crack tip is defined by the full configuration, including the nominal applied stress and the total crack length. Considering the defect sizes under consideration and the reduced range of short cracks estimated (100 μm according to the Chapetti model and 50 μm according to the Murakami-Endo model), it can be considered that the cracks will behave as long cracks very quickly.

In the case of $R = 0.1$, the estimated $\Delta\sigma_{eR}$ (fatigue limit) and ΔK_{dR} (minimum threshold for crack growth), and the measured ΔK_{thR} (threshold for long crack), are 1100 MPa, 2.83 MPa.m$^{1/2}$ and 5 MPa.m$^{1/2}$, respectively. The short crack range for this case is even shorter, and the threshold is fully developed for crack lengths of about 50 μm.

3.2. Near-surface crack growth resistance for the spring leaves

In this analysis, we consider the possibility of fracture occurring in the springs due to either superficial or subsuperficial defects. Shot peening introduces residual stresses with an uneven distribution, resulting in a load ratio R that varies with the crack length due to its superposition with the applied nominal stress distribution. Prior studies indicate that effective crack propagation for low or negative load ratios is influenced by a threshold value of K_{max}, referred to as $K_{max,th}$. Consequently, we utilize the parameter $K_{max,th}$ to estimate the fatigue limit as a function of the crack length (defect size). Additional information on this topic can be found in references [29–31].

The propagation threshold can be estimated by employing Eq. (1) and substituting ΔK with K_{max} as the analyzed parameter. To obtain this estimation, input data such as the long crack fatigue threshold in terms of K_{max} ($K_{max,th}$) and the fatigue limit in terms of stress amplitude ($\sigma_{e,max}$) are needed. The $K_{max,th}$ value can be obtained from the long crack growth fatigue test at a load ratio $R = 0.1$, as discussed in section 2.3, and it is determined to be 5.6 MPa.m$^{1/2}$.

On the other hand, it is necessary to obtain the resulting K_{res} due to the distribution of residual stresses as a function of the distance from the surface (crack depth). This was done using the stress distribution shown in Figure 4 and the weight functions reported by Shen *et al*. for a semicircular surface crack [32].

Figure 8 shows the estimated propagation threshold as a function of the parameter $K_{max,th}$, the applied K_{max} for a maximum applied stress of 1330 MPa, the K_{res} due to the residual stresses, and the total applied K_T obtained by summing K_{max} and K_{res}. It can be seen that the total K_T is similar to the $K_{max,th}$ for crack lengths up to about 0.3 mm. This suggests that defects on the surface or near-surface of the component with sizes smaller than this value would not lead to component failure. Therefore, it can be concluded that it is highly unlikely for the component to fail due to fracture initiated from surface or near-surface defects.

3.3. Fatigue cracks growth for internal cracks. Δσ-N curves estimation procedure for the spring leaves

Here, the fatigue resistance for crack initiation from internal defects is analyzed. In the six tests conducted on leaves and reported in section 2.5, the applied ΔK needs to be quantified by considering only the nominal stress distribution applied in bending. This is done by assuming that the cracks initiated during the process are circular in shape, with a diameter equal to the maximum dimension of the defect in the plane perpendicular to the nominal applied stresses. Furthermore, the locally applied nominal stress at the center of the defect is taken into consideration when calculating the applied ΔK. The crack propagation threshold considered is the same as the long crack threshold, ΔK_{thR}, because the defect sizes responsible for the six fractures are similar to or greater than 0.1 mm. This crack length falls within the range for which the short crack threshold has already been developed, as estimated in section 3.1.

Quantitative estimations of fatigue crack growth require to establish a constitutive relationship between the fatigue crack growth rate, *da/dN*, and the range of the applied stress intensity factor, ΔK. This relationship must also account for the threshold for fatigue crack growth. Among others, the following one meets these requirements [13, 14, 22]:

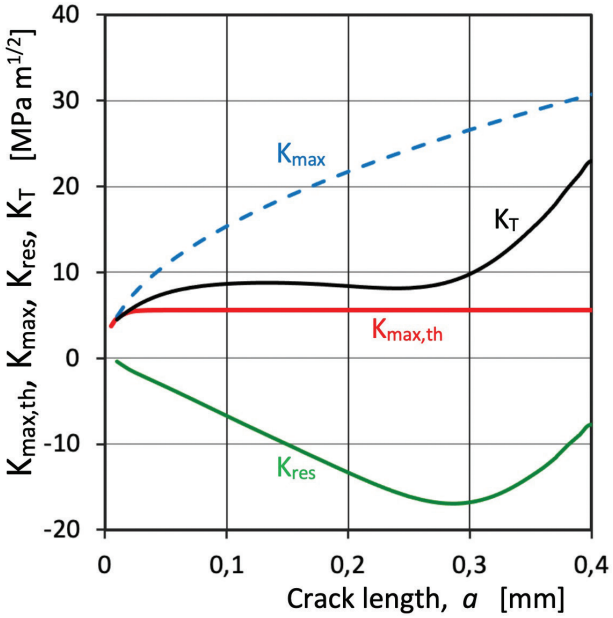

Figure 8: Threshold and applied curves as a function of crack length. Surface crack initiation with compressive residual stresses.

$$\frac{da}{dN} = C\left(\Delta K - \Delta K_{thR}\right)^m \tag{9}$$

where C and m are material and environmental constants and ΔK_{thR} is the fatigue threshold for long cracks. All of them obtained from long crack fatigue experimental results reported in section 2.3: C = 5.10^{-7} mm/cycle, m = 2.2 and ΔK_{thR} = 5.1 MPa.m$^{1/2}$ for R = 0.1. The da/dN vs ΔK function given by Eq. (9) is indicated by a red line in Figure 3.

The fatigue crack propagation life from an initial crack length a_i to a critical crack length a_f can be calculated by integrating Eq. (9). For the purpose of estimating fatigue resistance ($\Delta\sigma$ vs N curves), the initial crack length a_i is assumed to be the radius of a circular crack that encompasses the entire defect, while the final crack length a_f is set at 3 mm, which is the average value observed for the subcritical crack propagation zone on the fracture surfaces of the tested leaves, as shown in Figure 6.

To investigate the effect of defect size and depth on fatigue limit, the data from the six tests were analyzed. The fatigue limit was estimated as a function of depth D and initial crack length a_i. The results are shown in Figure 9, where the red solid circles represent the estimated fatigue limit for the six tests conducted. The estimated fatigue limit was also calculated for defect sizes corresponding to initial crack lengths of a_i = 0.05, 0.075, 0.1, 0.15, 0.2 and 0.3 mm. The observed defect sizes (diameter) $2a_i$ in the tests were in the range of 0.09 to 0.2 mm, and the depth ranged from 3 to 6 mm.

The results show the great dispersion that could be expected in terms of fatigue resistance if the statistical distribution of defect size and location are taken into account, being able to expect substantial increases in resistance if the maximum expected defect sizes were decreased.

The methodology used in this study enables the estimation of $\Delta\sigma$ vs N curves for various combinations of defect size and depths. As depicted in Figure 10, we present the estimated $\Delta\sigma$-N curves for six different scenarios, where the defect sizes a_i are 0.05, 0.1, and 0.2 mm, and depths D are 3 mm (indicated by black lines) and 6 mm (indicated by red dashed lines). In addition, the figure also displays the experimental results obtained from testing spring leaves under a nominal applied stress range $\Delta\sigma$ of 1200 MPa (represented by symbols). It is worth noting that the estimated fatigue limit for these tests falls within the range of 500–1000 MPa.

The estimations provided by the proposed methodology are both conservative and acceptable, as they are able to account for the relative differences observed experimentally. Additionally, the approach allows for the thorough analysis and quantification of the impact of the size and position of the initiating defect, enabling statistical analyses and investigations into the most unfavorable conditions, such as the minimum expected resistance values.

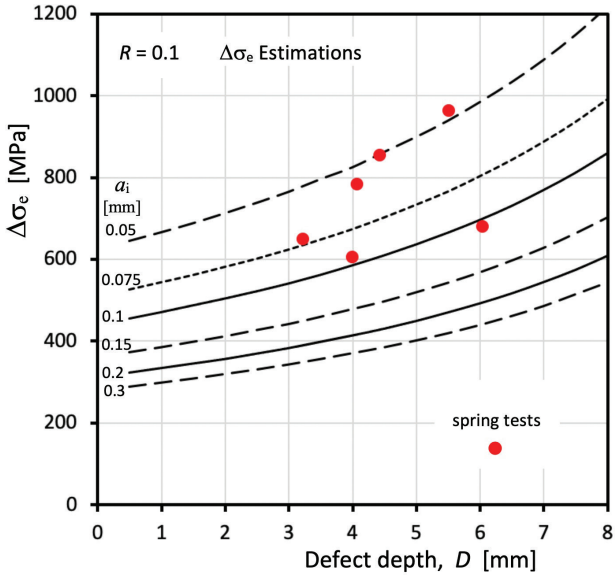

Figure 9: Estimated fatigue endurance (for 2.10^6 cycles) as a function of the position of the crack initiation (depth D), for different initial crack lengths a_i. Estimations for the six experiments are also shown (red symbols).

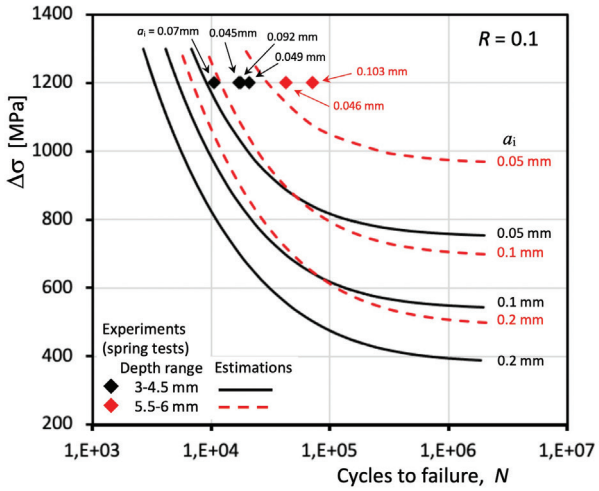

Figure 10: Estimated fatigue endurance (for 2.10^6 cycles) as a function of the position of the crack initiation (depth D), for different initial crack lengths a_i.

4. CONCLUDING REMARKS

The aim of this study was to investigate fatigue failure of a parabolic spring made of 51CrV4 steel. A fracture mechanics approach was applied to estimate and analyze the fatigue resistance of the spring, comparing the estimations with the experimental results. The analysis involved quantifying the applied driving force and resistance for various loading configurations, inclusion sizes, and residual stresses. Specifically, surface and internal initiation processes were analyzed, taking into account the impact of residual stresses introduced by shot peening in the former case.

Through the analysis, several key findings were identified, including:

– The ability of the methodology to analyze the influence of the different variables involved in the definition of the fatigue resistance and the configuration failure.
– The fracture process occurs due to the interplay of two competing fracture mechanisms: one that initiates on the surface and another that originates internally. By employing appropriate methodologies, these fracture processes can be quantified and compared.

– It seems that for the analyzed configuration, the variable to be optimized in the processing of the springs is the maximum size of the expected defect. Decreasing this maximum inclusion size would substantially increase the fatigue resistance of the parabolic spring, and the improvement can be quantified.
– The employed methodology facilitates not only the quantification but also the comprehension of the influence of the intrinsic material resistance on the fracture process.
– The analysis reveals that enhancing the propagation threshold for long cracks is a crucial factor in the quest to enhance spring resistance. Although steel strength increment typically lowers this threshold, exploring the option of increasing the microstructural size associated with the threshold definition process could lead to improvements. This process is often linked with the tortuosity or roughness resulting from the crack tip propagation process.

5. DECLARATION OF COMPETING INTEREST

The author declare that he has no known competing financial interests or personal relationships that could have appeared to influence the work reported in this paper.

6. ACKNOWLEDGMENTS

Author wishes to express his gratitude to the funding provided by Agencia Nacional de Promoción Científica y Tecnológica, Argentina (PICT 2017 Nro. 0982).

7. BIBLIOGRAPHY

[1] CEYHANLI, U.T., BOZCA, M., "Experimental and numerical analysis of the static strength and fatigue life reliability of parabolic leaf springs in heavy commercial trucks", *Advances in Mechanical Engineering*, v. 12, n. 7, pp. 1–17, 2020. doi: http://dx.doi.org/10.1177/1687814020941956

[2] FRAGOUDAKIS, R., SAIGAL, A., SAVAIDIS, G., *et al*., "Fatigue assessment and failure analysis of shot-peened leaf springs", *Fatigue & Fracture of Engineering Materials & Structures*, v. 36, n. 2, pp. 92–101, 2013. doi: http://dx.doi.org/10.1111/j.1460-2695.2011.01661.x

[3] SAVAIDIS, G., RIEBECK, L., FEITZELMAYER, K., "Fatigue life improvement of parabolic leaf springs", *Materials Testing*, v. 41, n. 6, pp. 234–240, 1999. doi: http://dx.doi.org/10.1515/mt-1999-410606

[4] AGRAWAL, M.L., AGRAWAL, V.P., KHAN, R.A., "A stress approach model for prediction of fatigue life by shot peening of EN45A spring steel", *International Journal of Fatigue*, v. 28, n. 12, pp. 1845–1853, 2006. doi: http://dx.doi.org/10.1016/j.ijfatigue.2005.12.004

[5] WANG, S., LI, Y., YAO, M., *et al*., "Compressive residual stress introduced by shot peening", *Journal of Materials Processing Technology*, v. 73, n. 1–3, pp. 64–73, 1998. doi: http://dx.doi.org/10.1016/S0924-0136(97)00213-6

[6] FARRAHI, G.H., LEBRUN, J.L., COURATIN, D., "Effect of shot peening on residual stress and fatigue life of a spring steel", *Fatigue & Fracture of Engineering Materials & Structures*, v. 18, n. 2, pp. 211–220, 1995. doi: http://dx.doi.org/10.1111/j.1460-2695.1995.tb00156.x

[7] GUBELJAK, N., PREDAN, J., *Determination of dynamic strength of spring steel bellow yield stress*, Maribor, Slovenia, University of Maribor, 2005. Industrial report for Štore Steel d.o.o. (in slovene).

[8] ŠTORE STEEL, Štore *Steel: company report about testing of springs, by spring producer*, Štore, Slovenia, Štore Steel d.o.o., Nov. 2008.

[9] GUBELJAK, N., CHAPETTI, M.D., PREDAN, J., *et al*., "Variation of fatigue threshold of sprong steel with pre-stressing", *Procedia Engineering*, v. 10, pp. 3339–3344, 2011. doi: http://dx.doi.org/10.1016/j.proeng.2011.04.551

[10] CHAPETTI, M.D., VUHERER, T., GUBELJAK, N., "Fatigue crack growth in 51CrV4 spring steel", In: *Proceedings of the XX Congreso Internacional de Materiales, SAM-CONAMET 2022*, Mar del Plata, Argentina, May 2022.

[11] AMERICAN SOCIETY FOR TESTING AND MATERIALS, *ASTM E647 Standard Test Method for Measurement of Fatigue Crack Growth Rates*, New Jersey, West Conshohocken, Wiley, 2015.

[12] INTERNATIONAL ORGANIZATION OF STANDARDIZATION, ISO 12108 *Metallic Materials - Fatigue Testing - Fatigue Crack Growth Method*, Geneva, ISO, 2018.

[13] FUCHS, H.O., *Metal fatigue in engineering*, 1st ed., New York, John Wiley and Sons Inc, 1980.

[14] SCHIJVE, J., *Fatigue of structures and materials*, Netherlands, Springer, 2009. doi: http://dx.doi.org/10.1007/978-1-4020-6808-9

[15] SCURACCHIO, B.G., BATISTA DE LIMA, N., SCHÖN, C.G., "Role of residual stresses induced by double peening on fatigue durability of automotive leaf springs", *Materials & Design*, v. 47, pp. 672–676, 2013. doi: http://dx.doi.org/10.1016/j.matdes.2012.12.066

[16] MILLER, K.J., DE LOS RIOS, E.R., *The behaviour of short fatigue cracks*, United Kingdom, EGF (ESIS), 1986.

[17] TANAKA, K., NAKAI, Y., YAMASHITA, M., "Fatigue growth threshold of small cracks", *International Journal of Fracture*, v. 17, n. 5, pp. 519–533, 1981. doi: http://dx.doi.org/10.1007/BF00033345

[18] TANAKA, K., AKINIWA, Y., "Resistance curve method for predicting propagation threshold of short fatigue cracks at notches", *Engineering Fracture Mechanics*, v. 30, n. 6, pp. 863–876, 1988. doi: http://dx.doi.org/10.1016/0013-7944(88)90146-4

[19] CHAPETTI, M.D., "Fatigue propagation threshold of short cracks under constant amplitude loading", *International Journal of Fatigue*, v. 25, n. 12, pp. 1319–1326, 2003. doi: http://dx.doi.org/10.1016/S0142-1123(03)00065-3

[20] MURAKAMI, Y., ENDO, M., "Effects of defects, inclusions and inhomogeneities on fatigue strength", *International Journal of Fatigue*, v. 16, n. 3, pp. 163–182, 1994. doi: http://dx.doi.org/10.1016/0142-1123(94)90001-9

[21] MURAKAMI, Y., *Metal fatigue: effect of small defects and nonmetallic inclusions*, 2nd ed., USA, Elsevier, 2019.

[22] MOLINA, C.A., CHAPETTI, M.D., "Estimation of high cycle fatigue behaviour using a threshold curve concept", *International Journal of Fatigue*, v. 125, pp. 23–34, 2019.

[23] CHAPETTI, M.D., "Fracture mechanics for fatigue design of metallic components and small defect assessment", *International Journal of Fatigue*, v. 154, pp. 106550, 2022. doi: http://dx.doi.org/10.1016/j.ijfatigue.2021.106550

[24] CHAPETTI, M.D., "A simple model to predict the very high cycle fatigue resistance of steels", *International Journal of Fatigue*, v. 33, n. 7, pp. 833–841, 2011. doi: http://dx.doi.org/10.1016/j.ijfatigue.2010.12.010

[25] MCEVILY, J., EIFLER, D., MACHERAUCH, E., "Analysis of the growth of short fatigue cracks", *Engineering Fracture Mechanics*, v. 40, n. 3, pp. 571–584, 1991. doi: http://dx.doi.org/10.1016/0013-7944(91)90151-P

[26] ZERBST, U., VORMWALD, M., PIPPAN, R., *et al*., "About the fatigue crack propagation threshold of metals as a design criterion - a review", *Engineering Fracture Mechanics*, v. 153, pp. 190–243, 2016. doi: http://dx.doi.org/10.1016/j.engfracmech.2015.12.002

[27] HU, Y.N., WU, S.C., WITHERS, P.J., *et al*., "The effect of manufacturing defects on the fatigue life of selective laser melted Ti-6Al-4V structures", *Materials & Design*, v. 192, pp. 108708, 2020. doi: http://dx.doi.org/10.1016/j.matdes.2020.108708

[28] LEONETTI, D., MALJAARS, J., SNIJDER, H.H., "Fracture mechanics based fatigue life prediction for a weld toe crack under constant and variable amplitude random block loading - modelling and uncertainty estimation", *Engineering Fracture Mechanics*, v. 242, pp. 107487, 2021.

[29] SADANANDA, K., VASUDEVAN, A.K., "Crack tip driving forces and crack growth representation under fatigue", *International Journal of Fatigue*, v. 26, n. 1, pp. 39–47, 2004. doi: http://dx.doi.org/10.1016/S0142-1123(03)00105-1

[30] VASUDEVAN, A.K., SADANANDA, K., "Analysis of crack growth under compression-compression loading", *International Journal of Fatigue*, v. 23, pp. S365–S374, 2001. doi: http://dx.doi.org/10.1016/S0142-1123(01)00172-4

[31] SADANANDA, K., SARKAR, S., "Modified Kitagawa diagram and transition from crack nucleation to crack propagation", *Metallurgical and Materials Transactions. A, Physical Metallurgy and Materials Science*, v. 44, n. 3, pp. 1175–1189, 2013. doi: http://dx.doi.org/10.1007/s11661-012-1416-x

[32] SHEN, G., PLUNTREE, A., GLINKA, G., "Weight function for the surface point of semi-elliptical surface crack in a finite thickness plate", *Engineering Fracture Mechanics*, v. 40, n. 1, pp. 167–176, 1991. doi: http://dx.doi.org/10.1016/0013-7944(91)90136-O